Polymer(Korea), Vol. 40, No. 2, pp. 265-274 (2016)
http://dx.doi.org/10.7317/pk.2016.40.2.265

ISSN 0379-153X(Print)
ISSN 2234-8077(Online)

산화구리와 탄소나노튜브가 실리콘 고무 나노복합재료의 열적 안정성에 미치는 영향

Qiang Zhang, Lu Bai, and Junping Zheng†

Tianjin Key Laboratory of Composite and Functional Materials, School of Materials Science and Engineering, Tianjin University

(2015년 10월 17일 접수, 2015년 12월 9일 수정, 2015년 12월 9일 채택)

Effects of Copper Oxide and Carbon Nanotubes on Thermal Stability of Silicone Rubber Nanocomposites

Qiang Zhang, Lu Bai, and Junping Zheng†

Tianjin Key Laboratory of Composite and Functional Materials, School of Materials Science and Engineering, Tianjin University, Tianjin 300072, P.R. China

(Received October 17, 2015; Revised December 9, 2015; Accepted December 9, 2015)

Abstract: Silicone rubber (SR) filled with carbon nanotubes (CNTs), copper oxide (CuO) and CuO modified CNTs (CuO-CNTs) were prepared to detect the effects of these additives on thermal stability of SR by thermogravimetric analysis and tensile testing before and after aging. Flynn-Wall-Ozawa method was also employed to analyze the thermal degradation kinetics. The results indicated that all the additives could increase the initial thermal degradation temperature and thermal oxidative aging properties of SR and a synergistic effect was found in CuO-CNTs/SR. Meanwhile, activation energies of SR filled with additives increased significantly relative to neat SR and found to be optimal for CuO-CNTs/SR with activation energy increasing to 231.29, 121.68 $kJ \cdot mol^{-1}$ larger than that of blank sample. It is because that CNTs and CuO could promote each other to capture the free radicals generated by thermal oxidative reaction of the methyl side groups and thereby terminate the process.

Keywords: silicone rubber, copper oxide, carbon nanotubes, thermal stability.

Introduction

Nowadays, polymer composites are more extensively applied in many industry fields. Using nano-size additives to modify polymers to obtain high performance nanocomposites has gained increasing attention in both academic and industrial areas, due to the significant improvement in terms of mechanical, thermal, electrical and catalytic properties.[1-5] For instance, some researches showed that the thermal stability and flame retardancy of polymers were improved after adding metal oxides, which were one of the most convenient and effective nano-size additives.[6-8]

Recently, with the widely application of the semiconductor technology, copper oxide (CuO), as a very important p-type semiconducting material, has drawn increasing research attention. The advantages of excellent sensing properties, narrow band gap, electrochemical activity, low production cost and abundant availability make CuO a high-performance nanoparticle and widely used in electrochemical and catalytic fields.[9-11] The studies of CuO/polymer composites are also mostly concentrated on the electrical properties.[12-14] In the past few years, several researches focused on the thermal properties have emerged.[6,15] For instance, Mazrouaa *et al*.[6] found that CuO nanopowders could improve the thermal stability of Poly o-anisidine, while Zhao *et al*.[15] thought that nano-CuO particles acted as a kind of catalyst which could decrease the thermal decomposition temperatures of the copolymer of 3,3'-bis(azidomethyl) oxetane and glycidyl azide polymer. There is almost no other related research and the opposite results above limit the application of CuO in the aspect of heat resistance in polymers. Therefore, further research concerning the effect of CuO on the thermal stability of some typical polymers remains to be investigated.

†To whom correspondence should be addressed.
E-mail: jpzheng@tju.edu.cn

Carbon nanotubes (CNTs) have received widespread attention since discovered by Iijima in 1991,[16] due to the excellent mechanical and thermal properties.[17] Some researches showed that CNTs could improve the thermal stability of polymers, such as silicone rubber (SR),[18,19] owing to its barrier and antioxidative effect. As an important modifier of CNTs, CuO modified CNTs (CuO-CNTs) have proved to have great application value in electric and photocatalysis fields.[20,21] It was because that CuO and CNTs could promote each other to have a good dispersion in the matrix and thus endow the composites with enhanced performance.[22] In view of the effects of CNTs and CuO on the thermal stability of some polymers and the interaction between CNTs and CuO in CuO-CNTs, polymers filled with CuO and CuO-CNTs may become novel high performance composites in the aspect of heat resistance.

Based on this purpose, in this study, SR which has outstanding thermal stability was chosen as matrix. CuO and CuO-CNTs were synthesized by precipitation method. Then the particles and CNTs were introduced into SR matrix to prepare nanocomposites. The characterizations of the additives were investigated by X-ray diffraction (XRD), Raman spectra, and transmission electron microscopy (TEM). Thermogravimetric analysis (TGA) and tensile testing before and after aging were employed to detect the effects of those nanoparticles on thermal stability of SR. In addition, an integral isoconversional method, Flynn-Wall-Ozawa (FWO) was utilized to analyze the activation energies of thermal degradation.

Experimental

Materials. Methylvinyl silicone gum (110-2; M_n, 5.0×10^5~7.0×10^5; vinyl group content, 0.15~0.18 mol%) was purchased from Bluestar Chengrand Chemical Co. Ltd. (Chengdu, China). Carboxylic CNTs (carboxyl ratio, 2.56 wt%; purity, >95%; diameter, 5-15 nm; length, 0.5-2 μm) were purchased from Chengdu Organic Chemicals Co. Ltd. Chinese academy of science (China). Fumed silica (AS-380) was purchased from Shenyang Chemical Co. Ltd. (China). Hexamethyldisilazane, polyvinylsiloxane and 2,5-*bis*(tertbutylperoxy)-2,5-dimethylhexane (DBPMH) were all industrial products and used as received. Other reagents were all of analytical reagents and used as obtained.

Preparation of CuO, CuO-CNTs and the Control CNTs Nanoparticles. Firstly, $Cu(NO_3)_2\cdot3H_2O$ (1.50 g) was added into absolute ethanol (200 mL), and stirred at 60 ºC until it was dissolved completely. Subsequently, carboxylic CNTs (0.30 g) were added into the above solution and the achieved mixture was sonicated for 3 h. Then surfactant sodium dodecylbenzenesulfonate (0.32 g) was added into the solution and stirred, later, sodium hydroxide (NaOH) aqueous solution was added as gelation agent drop by drop with continuous stirring at 60 ºC for 1 h. Finally, the obtained mixture was filtered, washed with deionized water for several times and then vacuum-dried at 60 ºC for 72 h. The calcination of this powder was performed at 350 ºC in a muffle furnace under argon atmosphere for 5 h, and followed by annealed to obtain CuO-CNTs nanoparticle. CuO was prepared following the same procedure above without adding CNTs at the beginning. To be used as a control additive, carboxylic CNTs was also calcined at 350 ºC in a muffle furnace under argon atmosphere for 5 h, and then annealed.

Preparation of SR Based Nanocomposites. Materials were milled on a two-roll mill (SR-160B, Guangdong Zhanjiang Machinery Factory, China). Firstly, 100 phr (parts per hundreds of rubber) of silicone gum was encapsulated onto rollers. 40 phr of fumed silica, 10 phr of hexamethyldisilazane, 2.6 phr of polyvinylsiloxane were mixed in step by step. After milled for 15 min, 3 phr of the prepared nanoparticles including CNTs, CuO and CuO-CNTs were added into the matrix, respectively. After milled uniformly, 0.7 phr of DBPMH was added. Finally, the mixture was cured in a stainless steel mold at 180 ºC under a pressure of 10 MPa for 10 min, and post-cured at 200 ºC for 4 h under ambient pressure for cross-linking. Thus, four kinds of nanocomposites named blank, CNTs/SR, CuO/SR and CuO-CNTs/SR were obtained.

Thermal Oxidative Aging Experiment. The vulcanizates above were aged in an air-blowing oven at 300 ºC for 12 h.

Crystallization Property and Purity of the Nanoparticles. X-ray diffraction (XRD) measurement was performed with a Rigaku DMAX-RC diffractometer (Japan) to determine the crystallization property and purity of the nanoparticles. Cu Kα radiation (λ=0.15406 nm) was used and scanning rate was $2^o\cdot min^{-1}$ with a generator voltage of 45 kV and a generator current of 180 mA. XRD peaks were collected from 2θ=20º to 80º. Raman spectra were measured in the range of 2000-500 cm^{-1} at ambient temperature on a DXR Raman microscope with an argon-ion laser beam of 532 nm wavelength.

Morphologies of the Nanoparticles. Transmission electron microscopy (TEM, Tecnai G2 F20, Philips) was employed to observe the morphologies of CuO and CuO-CNTs. The samples were prepared by dropping a sample suspension in ethanol on a Cu grid coated with a carbon film.

Thermal Stability of the SR Based Nanocomposites. Thermogravimetric analysis (TGA) was carried out using a Netzsch STA449F3 instrument (Germany). The nanoparticles were heated from ambient temperature to 900 °C at a heating rate of 10 °C·min^{-1} under air to determine the loading of CuO in the CuO-CNTs. The SR based nanocomposites were heated from ambient temperature to 700 °C at various heating rates of 5-20 °C·min^{-1} under air.

Tensile Testing. The tensile testing was performed on a universal testing machine (M350-20KN, Testometric, UK) at a 500 mm·min^{-1} cross-head speed at room temperature. The dumbbell-shaped specimens were obtained from vulcanized sheet. At least three specimens were tested for each sample and the mean value was reported.

Results and Discussion

Characterization of Prepared Nanoparticles. XRD measurement was used to determine the crystallization property and purity of nanoparticles. Figure 1 presents the XRD patterns of (a) CNTs, (b) CuO, and (c) CuO-CNTs. Two diffraction peaks at 2θ=26.1° and 42.7° can be attributed to the (002) and (100) reflections of CNTs, respectively. The diffraction peaks of CuO at 2θ=32.7°, 35.7°, 38.9°, 49.1°, 53.6°, 58.5°, 61.3°, 66.6°, 68.3°, 72.4° and 75.3° correspond to the (110), (002), (111), ($\bar{2}$02), (020), (202), ($\bar{1}$13), ($\bar{3}$11), (220), (311) and ($\bar{2}$22) reflections of CuO. There are no other peaks of impurity in the pattern (b), and the peaks are sharp, which show the excellent crystallization property and high purity of CuO. Similar peaks with those of CuO can be found on the XRD pattern of CuO-CNTs, and the diffraction peaks at 2θ=26.1° and 42.7° are the (002) and (100) reflections of CNTs, which are similar to those of pattern (a).

In order to further confirm the presence of CuO on the surface of CNTs, Raman analysis was carried out (Figure 2). Both the two samples present two main peaks at about 1342 and 1576 cm^{-1}, which are associated with the D-band and G-band of multiwall CNTs,[23] respectively. The ratio of the intensity of D-bands to G-bands (I_D/I_G) can suggest the defect density of CNTs materials,[24] and then it can be determined that whether the CuO modifies on the surface of CNTs. As shown in Figure 2, I_D/I_G is 1.12 for the CNTs and then increases to 1.28 after CuO loading. This phenomenon is consistent with the previous research[25] that the metal oxides loading can damage the order of the graphite layers of CNTs and increase the concentration of defects.

In conclusion, according to XRD and Raman analyses, CuO was successfully attached onto the surface of CNTs.

The morphologies of CuO and CuO-CNTs were given by TEM observations. Figure 3 shows TEM photographs of (a) CuO, (b) CuO-CNTs with low resolution and (c) CuO-CNTs with high resolution. Figure 3(a) shows irregular shape and aggregation of CuO, whose mean particle sizes are more than 60 nm. Differently, in Figure 3(b), it can be seen that the diameter of the spherical CuO on the surface of CNTs is nearly 10 nm and the CuO nanoparticles distribute uniformly and combine closely with CNTs. This phenomenon means that the special surface area of CuO in the CuO-CNTs is enlarged. Figure 3(c) shows the obvious lattice fringe with the fringe spacing being 0.2324 nm, corresponding to the (111) reflection of

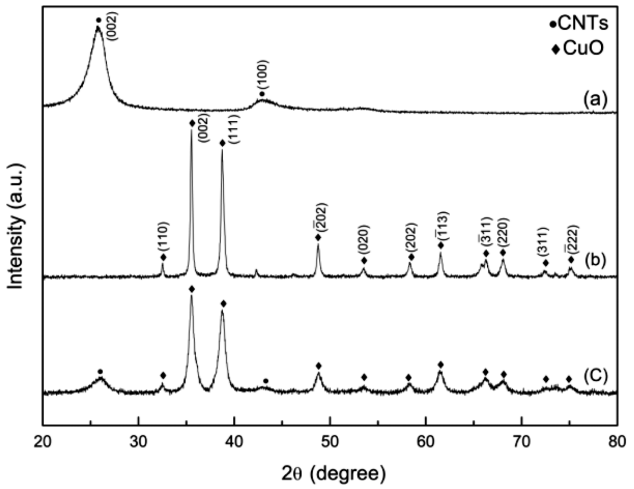

Figure 1. XRD patterns of (a) CNTs; (b) CuO; (c) CuO-CNTs.

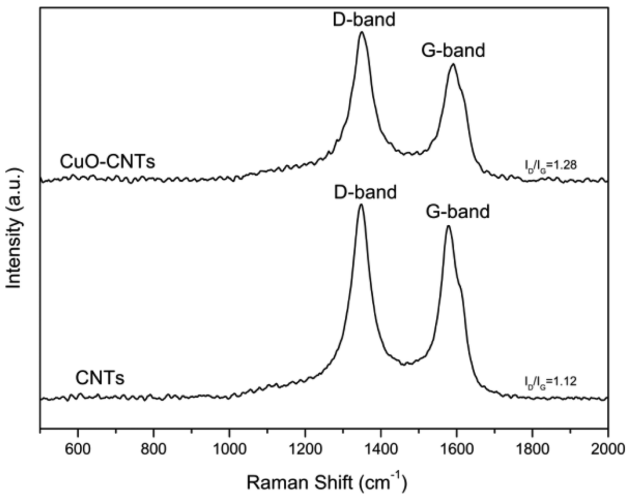

Figure 2. Raman spectra of CNTs and CuO-CNTs.

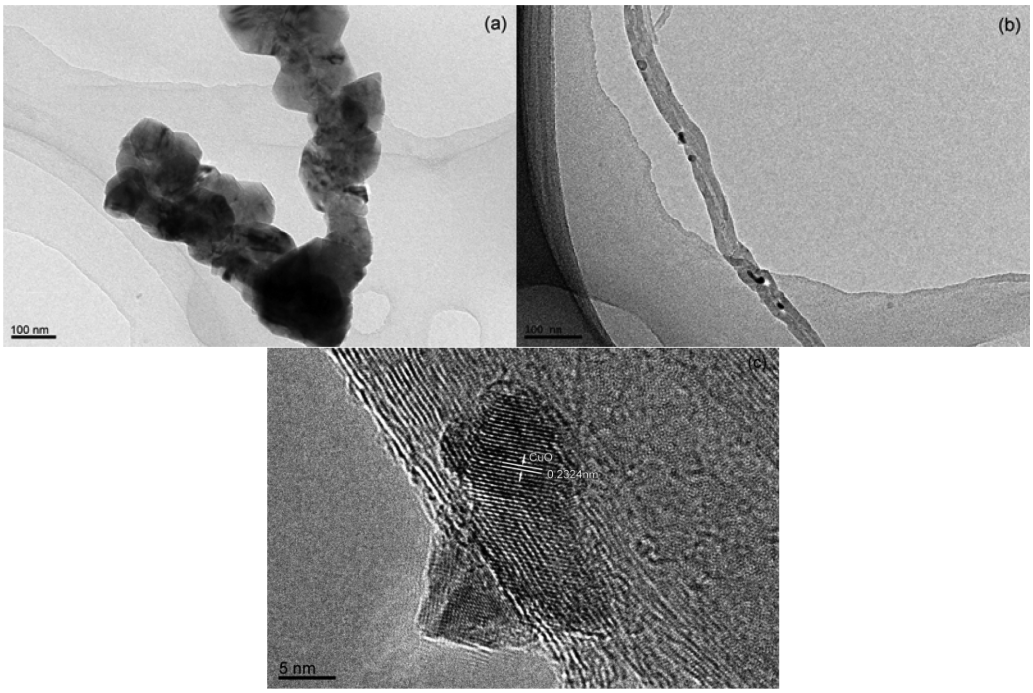

Figure 3. TEM images of (a) CuO; (b) CuO-CNTs with low resolution; (c) CuO-CNTs with high resolution.

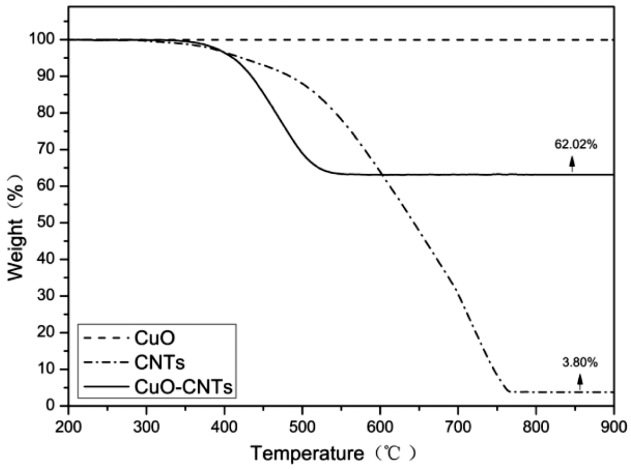

Figure 4. TGA curves of CNTs, CuO and CuO-CNTs.

CuO. It indicates that the particles attached on the surface of CNTs are really well-crystallized CuO.

In order to estimate the content of CuO in the CuO-CNTs, TGA was carried out under air, as shown in Figure 4. It can be seen that the CuO remains thermally stable when heated to 900 ºC, while the CuO-CNTs starts to decompose at about 350 ºC until weight remains 62.02% of the initial weight and CNTs nearly burn out at about 760 ºC. Since the CuO remains stable in this temperature range, any weight loss corresponds to the oxidation of CNTs. Therefore, the change in weight before and after the oxidation of CNTs can be translated into the content of CuO in the CuO-CNTs. By this method, the content of CuO attached on CNTs is determined to be about 58.22%.

Dispersion of CNTs and CuO-CNTs in SR Based Nanocomposites. Figure 5 shows the SEM images of CNTs/SR and CuO-CNTs/SR. The dark fields represent SR matrix, and the obviously bright fields are the embedded CNTs (Figure 5(a)) and CuO-CNTs (Figure 5(b)). It can be clearly seen from the Figure 5(a) that there are obvious aggregations of CNTs in CNTs/SR nanocomposite, while CuO-CNTs are well dispersed into the matrix. Owing to the attachment of CuO, the inter-tube spacing increases and the van der Waals interaction between the CNTs decreases markedly. Thus the dispersion of CuO-CNTs in the SR matrix is improved.

Thermal Oxidative Aging Properties of SR Based Nanocomposites. The mechanical properties of SR based nanocomposites before and after thermal oxidative aging are shown in Figure 6. As illustrated in Figure 6(a), before the thermal oxidative aging, the tensile strength of the samples with additives is slightly larger than that of the blank sample (around 5.51 MPa). But the difference between the CNTs/SR, CuO/SR and CuO-CNTs/SR is not obvious (around 5.76 MPa). However, after aging, the effects of the additives are significant. Blank sample was brittle and the tensile strength of that was too weak to be detected, while adding additives can

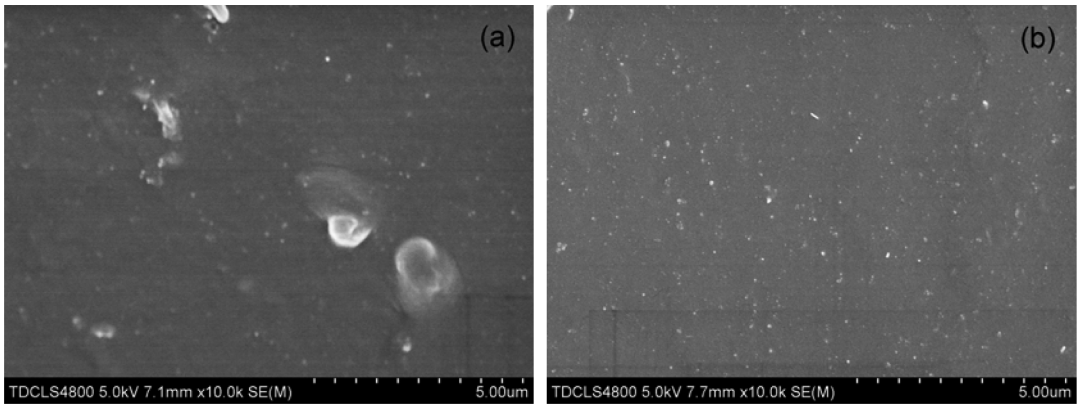

Figure 5. SEM images of (a) CNTs/SR; (b) CuO-CNTs/SR.

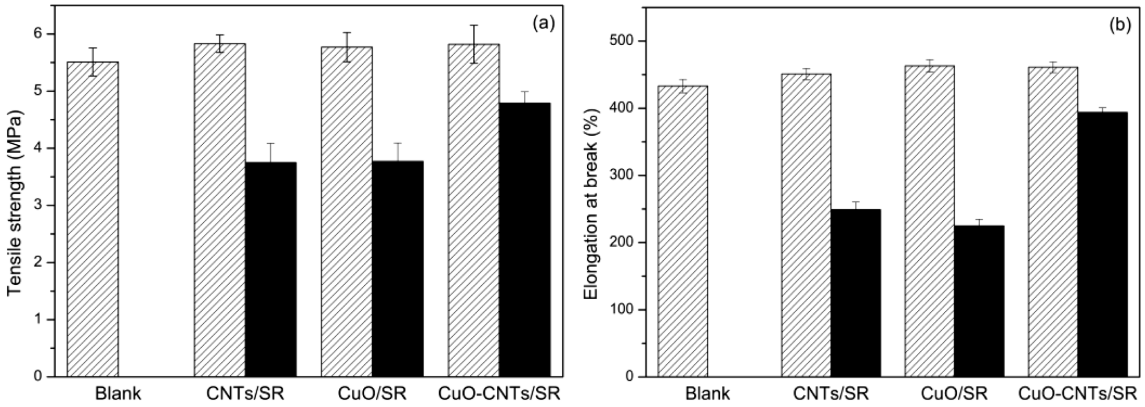

Figure 6. Mechanical properties of SR based nanocomposites before and after thermal oxidative aging (gray bar: before aging; blank bar: after aging): (a) tensile strength; (b) elongation at break.

remarkably improve the tensile strength of aged SR nanocomposites in varying degrees.

The tensile strength of aged CNTs/SR and CuO/SR are about 3.75 and 3.77 MPa, respectively. A notable enhancing effect is observed in CuO-CNTs/SR. The tensile strength of this aged sample is nearly 4.80 MPa, which is far higher than those of CNTs/SR and CuO/SR. Considering that the amount of CuO and CNTs in CuO-CNTs is respectively less than that of single CuO and CNTs, it can be concluded that the CuO and CNTs in CuO-CNTs have synergetic effect on enhancing the thermal oxidative aging properties of SR.

Similar results can be found on the changes of the elongation at break (Figure 6(b)). The improved thermal oxidative aging properties of CNTs/SR are owing to the excellent properties of CNTs.[18] As an effective antioxidant, CuO inhibits some reactions during the thermal oxidative aging process and thereby improves the mechanical properties of aged SR. The significant improvement of CuO-CNTs on the thermal oxidative aging properties of aged SR is attributed to the properties of CNTs, as well as the smaller size and better dispersion of CuO nanoparticles on the surface of CNTs, which give CuO an enlarged special surface area in CuO-CNTs. Therefore, the interaction between CuO nanoparticles and SR matrix can be improved significantly. And the effect of the CuO is amplified.

Thermal Stability of SR Based Nanocomposites. In order to further investigate the effects of these additives on the thermal stability of SR, it is necessary to perform TGA. Figure 7 shows the TGA and differential thermogravimetry (DTG) curves of SR based nanocomposites under air. Meanwhile, the details of mass loss data, including the onset degradation temperature T_{onset} (defined as the temperature for 1% mass loss), characteristic temperatures T_5, T_{20} and T_{50} (defined as the temperature for 5%, 20% and 50% mass loss, respectively) and the temperatures at peaks of DTG curves T_p, are summarized in Table 1.

Two major degradation peaks can be observed in the DTG

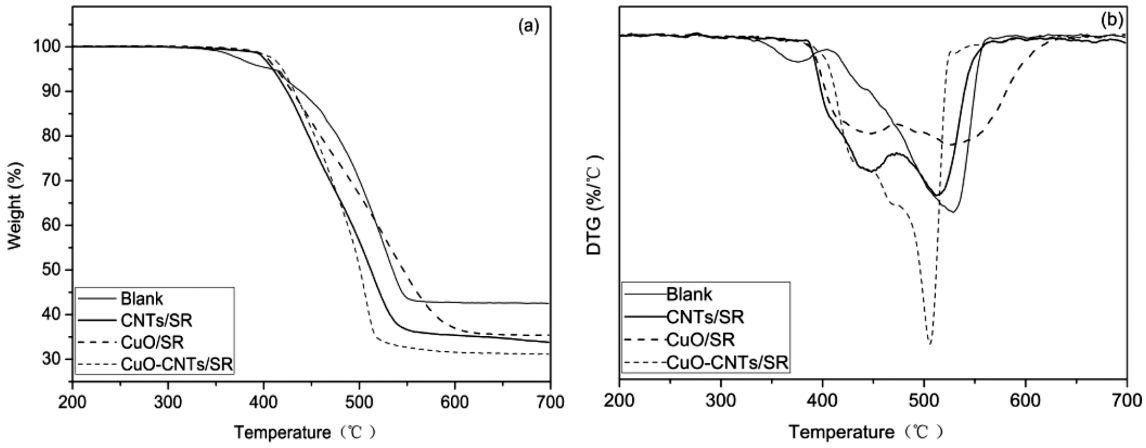

Figure 7. (a) TGA; (b) DTG curves of SR based composites at constant heating rate of 10 °C·min^{-1} under air.

Table 1. Characteristic Data Obtained from TGA and DTG Curves

Sample	T_{onset}(°C)	T_5(°C)	T_{20}(°C)	T_{50}(°C)	T_p(°C)	
					T_p^1(°C)	T_p^2(°C)
Blank	352	408	477	534	375	523
CNTs/SR	383	409	447	512	448	512
CuO/SR	390	413	459	546	444	527
CuO-CNTs/SR	386	422	454	501	-	506

curves (Figure 7(b)). According to the literatures,[26,27] the first thermal degradation stage is mostly due to the thermal oxidative reaction, involving the oxidization of methyl side groups and oxidative crosslinking. The second stage can be attributed to the thermal depolymerization of the main chain of SR. Therefore, the T_p^1 (temperature at the first peak of DTG curves) and the T_p^2 (temperature at the second peak of DTG curves) can stand for the thermal stability of the nanocomposites at the two stages.

It is obvious that the nanoparticles can significantly improve the thermal stability of SR at the first degradation stage. The blank sample gets a T_{onset} of about 352 °C and the addition of the additives increases the T_{onset} of SR nanocomposites in varying degrees. As an effective antioxidant, CuO has the radical scavenging ability to capture free radicals which are generated during the process of the oxidization and can catalyze the degradation of SR to cyclic oligomers.[26,27] Through this effect, the thermal oxidative reaction is inhibited effectively by CuO and thereby the thermal stability of CuO/SR is improved. For the improved thermal stability of CNTs/SR at this stage, CNTs has the barrier effect to decrease the mobility of SR.[18] And owing to the thermal conductivity, CNTs can form an effective thermal conducting network in the matrix, which can eliminate the local overheating of SR.[5] According to the literature,[28] CNTs also has the radical scavenging ability. When the mass loss is about 5%, the first degradation stage of blank sample has been already finished, while other samples are still at this step. Therefore, the T_5 of blank sample is meaningless at this stage. The T_5 of CNTs/SR and CuO/SR are 409 and 413 °C, respectively. CuO-CNTs/SR has the highest T_5 about 422 °C. Also, compared with that of blank sample, T_p^1 of CNTs/SR and CuO/SR are increased by 73 and 69 °C, respectively, which means that CNTs and CuO present an outstanding effect on improving the thermal stability of SR. It is worth mentioning that, in the DTG curve of CuO-CNTs/SR, there is almost no obvious peak can be observed at the first stage. The synergistic effect between CuO and CNTs mentioned above makes CuO-CNTs an excellent antioxidant to promote each other to capture the free radicals. Meanwhile, a better dispersion of CuO-CNTs in the SR matrix than that of CNTs, which can be seen from the Figure 5, makes the effect of CNTs play better. Therefore, the first thermal degradation stage of CuO-CNTs/SR has been suppressed significantly and the CuO-CNTs/SR has the best thermal stability among all the samples. This is consistent with the results of thermal oxidative aging properties testing, which is performed at a relatively low temperature (300 °C).

However, adding antioxidant additives can not only inhibit the oxidation of side methyl groups, but also restrain the oxidative crosslinking reaction. The oxidative crosslinking reaction can largely decrease the mobility of SR main chain and thereby delay the further depolymerization of the SR. Therefore, for the second thermal degradation stage which is dominated by the random main chain scission reaction, the thermal stability of the SR filled with CNTs, CuO and CuO-CNTs decreases. For example, the T_{20} of blank sample (477 °C) is 30, 18 and 23 °C higher than those of CNTs/SR, CuO/SR and CuO-CNTs/SR nanocomposites, respectively. Meanwhile, the CuO-CNTs/SR has the lowest T_{50} and T_p^2 (about 501 and 506 °C, respectively), which means that the greater the inhibition of oxidation at the first degradation stage is, the stronger the promotion of degradation of the SR main chain in the second degradation stage is. The TGA and DTG curves of CuO/SR indicate that the overall thermal degradation process of this sample is relatively flat and there is no rapid weight loss. In the late stage of thermal degradation, the thermal stability of this sample is a little better than others.

To summarize the analysis above, the first thermal degradation stage which is mostly due to the thermal oxidative reaction is effectively inhibited by the CNTs and CuO. It is because that the CNTs have the barrier and antioxidative effect, and CuO has the radical scavenging ability to capture free radicals generated during the process. CuO-CNTs/SR has the best thermal stability among the samples owing to the synergistic effect between CNTs and CuO. For the second degradation stage, because the oxidative crosslinking reaction, which can delay the further depolymerization of the SR main chain, has been restrained by the additives, the thermal stability of the CNTs/SR, CuO/SR and CuO-CNTs/SR decreases.

Activation Energies of Thermal Degradation of SR Based Nanocomposites. The activation energy (E) of thermal degradation is an exceedingly important kinetic parameter which can reflect the thermal stability of materials. Integral isoconversional methods are considered to be the most effective way to calculate the E, and the most frequently used one

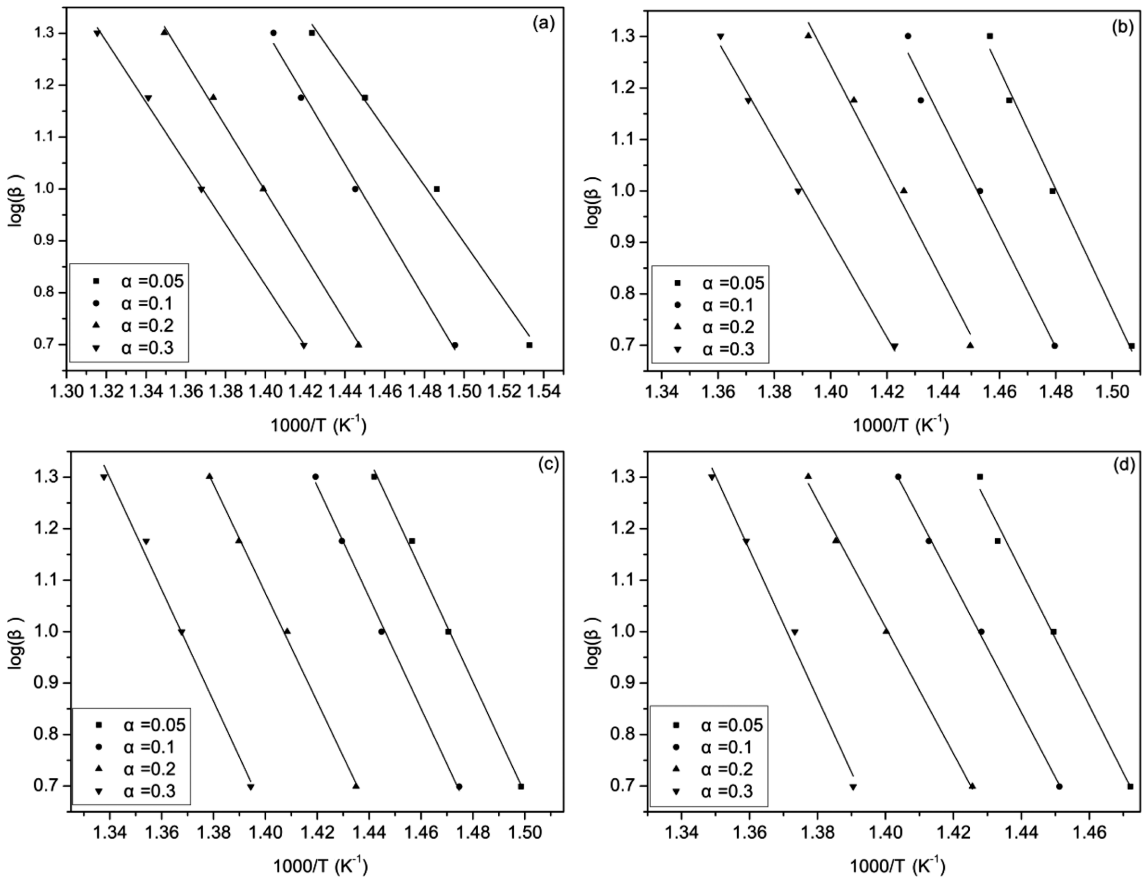

Figure 8. Activation energies obtained from FWO method at the first thermal degradation stage under air of (a) blank sample; (b) CNTs/SR; (c) CuO/SR; (d) CuO-CNTs/SR for the following degrees of conversion: α=0.05, 0.1, 0.2 and 0.3.

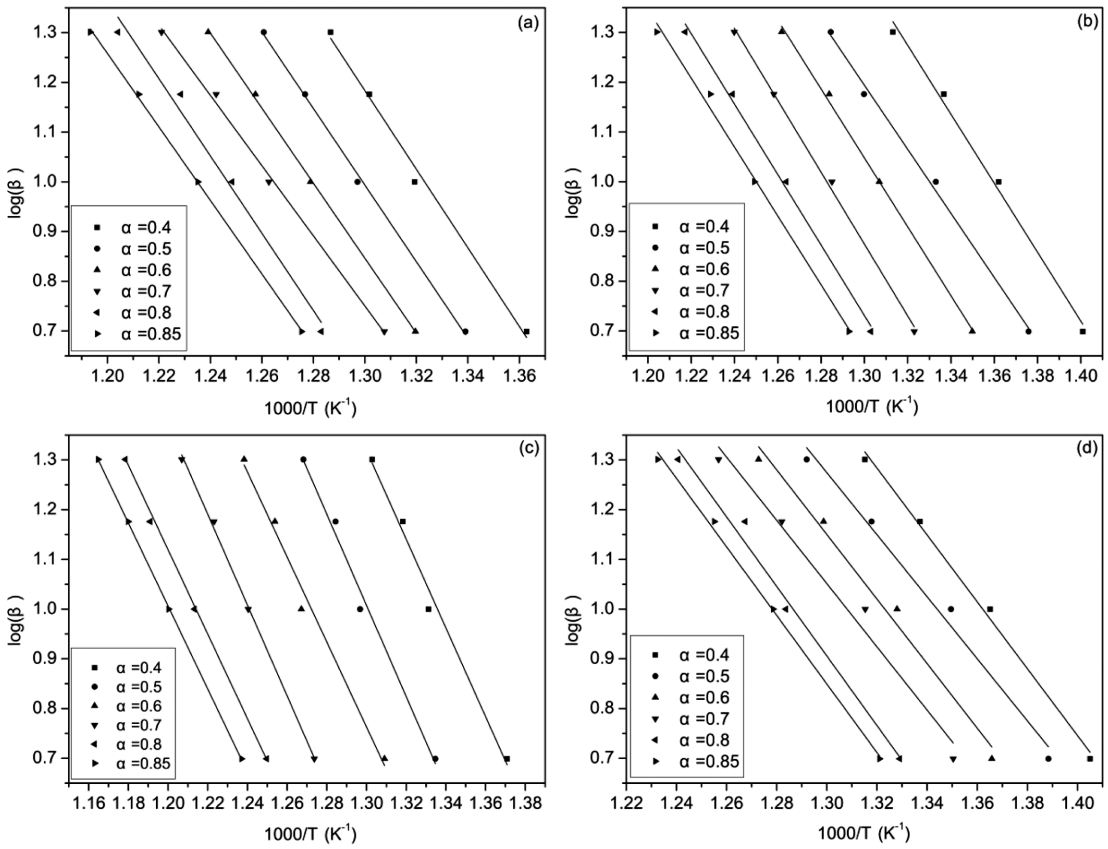

Figure 9. Activation energies obtained from FWO method at the second thermal degradation stage under air of (a) blank sample; (b) CNTs/SR; (c) CuO/SR; (d) CuO-CNTs/SR for the following degrees of conversion: α=0.4, 0.5, 0.6, 0.7, 0.8 and 0.85.

is Flynn-Wall-Ozawa (FWO) method.[29,30]

The degree of decomposition (α) can be defined as the following equation:

$$\alpha = (W_o - W_t)/(W_o - W_f) \quad (1)$$

where W_o, W_t and W_f are the initial, actual and final mass of the material, respectively. For a solid-state process, the decomposition kinetics can be described by the following general expression:

$$d\alpha/dt = k(T)f(\alpha) \quad (2)$$

where $d\alpha/dt$ is the decomposition rate, $f(\alpha)$, depending on the particular decomposition mechanism, is the function of α, T is Kelvin temperature, t is the time. And $k(T)=Aexp(-E/RT)$ stands for the Arrhenius rate constant. Under non-isothermal conditions with the constant heating rate $\beta(\beta=dT/dt)$, substituting the $k(T)$ into eq. (2), it can be obtained:

$$d\alpha/f(\alpha) = (A/\beta)\exp(-E/(RT))dT \quad (3)$$

where A is the pre-exponential factor, E is the activation energy, and R is the universal gas constant.

Table 2. Activation Energies at Two Thermal Degradation Stages of SR Based Nanocomposites

Sample	E (kJ·mol^{-1})			
	E_1	ΔE_1	E_2	ΔE_2
Blank	109.61	-	137.65	-
CNTs/SR	190.86	+81.25	126.01	-11.64
CuO/SR	195.96	+86.35	158.78	+21.13
CuO-CNTs/SR	231.29	+121.68	118.88	-18.77

ΔE stands for the value of E of composites filled with additives subtracting the E of the blank sample.

FWO method is an integral method which is based on:

$$G(\alpha) = \int_0^{\alpha} \frac{d\alpha}{f(\alpha)} = \frac{A}{\beta}\int_0^{T} \exp\left(-\frac{E}{RT}\right)dT \quad (4)$$

$$\log\beta = \log\left(\frac{AE}{RG(\alpha)}\right) - 2.315 - 0.4567\frac{E}{RT} \quad (5)$$

From eq. (5), $\log\beta$~1000/T is a straight line with slope coef-

ficient being -0.4567 *E/R*. Therefore, if a series of experiments are run at different values of β, the E can be obtained from a log β versus 1000/T plot. In this case, non-isothermal TGA of all SR nanocomposites with different heating rates of 5, 10, 15 and 20 $^{o}C \cdot min^{-1}$ were performed under air. The α=0.05, 0.1, 0.2 and 0.3 were chosen to evaluate the E of the first thermal degradation stage (E_1), and α=0.4, 0.5, 0.6, 0.7, 0.8 and 0.85 were chosen to evaluate the E of the second thermal degradation stage (E_2). Thus, several parallel lines were fitted, as shown in Figure 8 and Figure 9, respectively. And the values of E are illustrated in Table 2.

The E has a similar tendency with the results of TGA and DTG under air atmosphere. For the first thermal degradation stage, adding the nanoparticles does significantly improve the E_1. Blank sample gets the lowest E_1 of about 109.61 $kJ \cdot mol^{-1}$, while the values of CNTs/SR and CuO/SR are 81.25 and 86.35 $kJ \cdot mol^{-1}$ larger than that of blank sample. It's worth noting that the SR filled with CuO-CNTs has the largest E_1 among all the samples, which is about 231.29 $kJ \cdot mol^{-1}$ and is far larger than those of others. The results indicate that the additives can effectively increase the thermal stability of the SR nanocomposites at the first thermal degradation stage and the synergistic effect in CuO-CNTs is highly significant. These values corroborate the thermal oxidative aging properties results.

For the second thermal degradation stage, the E_2 of the blank sample is 137.65 $kJ \cdot mol^{-1}$, which is larger than those of CNTs/SR and CuO-CNTs/SR. CuO/SR nanocomposite has a slightly larger E_2 (158.78 $kJ \cdot mol^{-1}$) than others. The activation energy values and the results of TGA under air are consistent.

Conclusions

The effects of CNTs, CuO and CuO-CNTs on the thermal stability of SR based nanocomposites were systematically investigated. The results of TGA and DTG exhibit that CNTs and CuO can improve the thermal stability of the SR at the first degradation stage through inhibiting the oxidization of methyl side groups and oxidative crosslinking. It is because that CuO has the radical scavenging ability to capture free radicals and CNTs have the antioxidant ability. The synergistic effect is found in CuO-CNTs and makes CuO-CNTs/SR have the best thermal stability among all the samples: mechanical properties of aged CuO-CNTs/SR just decrease by about 15% during thermal oxidative aging; there are no obvious peaks can be observed at the first stage from the DTG curve of CuO-CNTs/SR, indicating the better antioxidant effect than CNTs and CuO; the E_1 of CuO-CNTs/SR is around 231.29 $kJ \cdot mol^{-1}$, which is far larger than those of others. Considering the SR is usually used at the corresponding temperature of the first stage, the CuO and CuO-CNTs may have potential applications in some fields.

Acknowledgements: This investigation was supported by the National Natural Science Foundation of China (Grant No. 51273143).

References

1. B. Pradhan and S. K. Srivastava, *Polym. Int.*, **63**, 1219 (2014).
2. Y. H. Yeom, H. Y. Na, and S. J. Lee, *Polym. Korea*, **38**, 767 (2014).
3. J. Munoz and M. Baeza, *Microchem. J.,* **122**, 189 (2015).
4. J-U. Ha, J. Hong, M. Kim, J. K. Choi, D. W. Park, and S. E. Shim, *Polym. Korea*, **37**, 722 (2013).
5. S. Sagar, N, Iqbal, A, Maqsood, M. Shahid, N. A. Shah, T. Jamil, and M. I. Bassyouni, *J. Compos. Mater.*, **49**, 995 (2015).
6. N. A. Mansour, M. G. Mohamed, A. M. Mazrouaa, and M. Y. Abed, *High Perform. Polym.*, **24**, 625 (2012).
7. X. Wang, W. Y. Xing, Y. Hu, X. M. Feng, B. Yu, H. D. Lu, and L. Song, *Chem. Eng. J.*, **250**, 214 (2014).
8. H. T. Ong, N. M. Julkapli, M. F. Tai, and S. B. Hamid, *J. Magn. Magn. Mater.*, **395**, 173 (2015).
9. M. Y. Chuai, Q. Zhao, and M. Z. Zhang, *Mater. Lett.*, **161**, 205 (2015).
10. S. E. Moosavifard, J. Shamsi, S. Kadkhodazade, and S. Fani, *Ceram. Int.,* **40**, 15973 (2014).
11. Y. Q. Wang, T. T. Jiang, J. Han, D. W. Meng, J. Yang, Y. C. Li, and Q. Ma, *Appl. Surf. Sci.,* **317**, 414 (2014).
12. B. B. Wang and L. X. Gu, *Mater. Lett.,* **57**, 361 (2002).
13. L. F. Yang, D. Q. Chu, and L. M. Wang, *Mater. Lett.*, **160**, 246 (2015).
14. R. Jiang, H. Y. Zhu, Y. J. Guan, Y. Q. Fu, L. Xiao, Q. Q. Yuan, and S. T. Jiang, *Chem. Eng. Technol.*, **34**, 179 (2011).
15. F. Q. Zhao, J. F. Pei, R. Z. Hu, X. D. Song, X. N. Ren, H. X. Gao, T. An, and J. An, *J. Anal. Appl. Pyrol.*, **112**, 88 (2015).
16. S. Iijima, *Nature*, **354**, 56 (1991).
17. R. H. Baughman, A. A. Zakhidov, and W. A. de Heer, *Science*, **297**, 787 (2002).
18. A. Katihabwa, W. C. Wang, Y. Jiang, X. Y. Zhao, Y. L. Lu, and L. Q. Zhang, *J. Reinf. Plast. Compos.,* **30**, 1007 (2011).
19. S. M. Shang, L. Gan, and M. C. Yuen, *Compos. Sci. Technol.,* **86**, 129 (2013).
20. D. W. Kim, K. Y. Rhee, and S. J. Park, *J. Alloy Compd.,* **530**, 6 (2012).
21. X. J. Zhang, W. H. Shi, J. X. Zhu, D. J. Kharistal, W. Y. Zhao, B. S. Lalia, H. H. Hng, and Q. Y. Yan, *ACS Nano*, **5**, 2013 (2011).

22. W. D. Zhang, B. Xu, and L. C. Jiang, *J. Mater. Chem.*, **20**, 6383 (2012).
23. M. Corrias, G. Dechambre, and J. L. Lacout, *Carbon*, **41**, 2361 (2003).
24. S. Q. Song, H. X. Yang, R. C. Rao, H. D. Liu, and A. M. Zhang, *Catal. Commun.*, **11**, 783 (2010).
25. J. A. Rodríguez-Manzo, O. Cretu, and F. Banhart, *ACS Nano*, **4**, 3422 (2012).
26. S. Hamdani, C. Longuet, F. Ganachaud, D. Perrin, and F. Ganachaud, *Polym. Degrad. Stab.*, **94**, 465 (2009).
27. G. Camino, S. M. Lomakin, and M. Lazzari, *Polymer*, **42**, 2395 (2001).
28. P. C. P. Watts, P. K. Fearon, and W. K. Hsu, *J. Mater. Chem.*, **13**, 491 (2003).
29. S. L. Tan, L. X Ma, X. D. Tang, and X. G. Sun, *High Perform. Polym.*, **27**, 65 (2015).
30. B. Li, Z. D. Zhang, D. P. Ma, Q. Q. Zhai, J. Zhang, and S. Y. Feng, *J. Appl. Polym. Sci.*, **132**, 41 (2015).